



# Reduced blood oxygenation level dependent connectivity is related to hypoperfusion in Alzheimer's disease

Jens Göttler<sup>1,2</sup> , Christine Preibisch<sup>1,2,3</sup> , Isabelle Riederer<sup>1,2</sup>, Lorenzo Pasquini<sup>2,4</sup>, Panagiotis Alexopoulos<sup>5</sup>, Karl Peter Bohn<sup>6</sup>, Igor Yakushev<sup>2,6</sup>, Ebba Beller<sup>7</sup>, Stephan Kaczmarz<sup>1,2</sup>, Claus Zimmer<sup>1</sup>, Timo Grimmer<sup>2,5</sup>, Alexander Drzezga<sup>6,8</sup> and Christian Sorg<sup>1,2,5</sup>

## Abstract

Functional connectivity of blood oxygenation level dependent signal fluctuations (BOLD-FC) is decreased in Alzheimer's disease (AD), and suggested to reflect reduced coherence in neural population activity; however, as both neuronal and vascular-hemodynamic processes underlie BOLD signals, impaired perfusion might also contribute to reduced BOLD-FC; 42 AD patients and 27 controls underwent simultaneous PET/MR imaging. Resting-state functional MRI assessed BOLD co-activity to quantify BOLD-FC, pulsed arterial spin labeling (pASL) assessed cerebral blood flow (CBF) as proxy for vascular hemodynamics, and <sup>18</sup>F-fluorodeoxyglucose PET assessed glucose metabolism (GluMet) to index neuronal activity. Patients' BOLD-FC, CBF, and GluMet were reduced within the same precuneal parietal regions. BOLD-FC was positively associated with mean CBF, specifically in patients and controlled for GluMet levels, suggesting that BOLD-FC reductions correlate with pASL-derived hypoperfusion in AD, independently from <sup>18</sup>F-fluorodeoxyglucose PET-derived hypometabolism. Data indicate that impaired vascular hemodynamic processes contribute to reduced BOLD connectivity in AD.

## Keywords

Alzheimer's disease, resting-state fMRI, blood oxygenation level dependent-functional connectivity, arterial spin labeling, <sup>18</sup>F-fluorodeoxyglucose-positron emission tomography

Received 15 July 2017; Revised 8 December 2017; Accepted 20 December 2017

## Introduction

Reductions in the functional connectivity of blood oxygenation level dependent signal fluctuations (BOLD-FC) in resting-state fMRI are consistent findings in Alzheimer's disease (AD), ranging from preclinical stages to mild cognitive impairment and dementia.<sup>1–3</sup> BOLD-FC is thought to reflect brain activity-dependent connectivity, which is considered relevant for both pathology spread along functional networks<sup>4,5</sup> and impact on brain organization<sup>6,7</sup> in AD. BOLD-FC changes are most consistently located in temporal and parietal regions of the posterior default mode network (pDMN) and typically interpreted as a loss of coherence in neuronal population activity.<sup>8,9</sup> Since the BOLD signal reflects the hemodynamic response to neuronal activity, it also highly depends

<sup>1</sup>Department of Diagnostic and Interventional Neuroradiology, Klinikum Rechts der Isar, Technische Universität München, Munich, Germany

<sup>2</sup>TUM Neuroimaging Center (TUM-NIC), Klinikum Rechts der Isar, Technische Universität München, Munich, Germany

<sup>3</sup>Clinic for Neurology, Klinikum Rechts der Isar, Technische Universität München, Munich, Germany

<sup>4</sup>Department of Neurology, Memory and Aging Center, University of California San Francisco, San Francisco, CA, USA

<sup>5</sup>Department of Psychiatry and Psychotherapy, Klinikum Rechts der Isar, Technische Universität München, Munich, Germany

<sup>6</sup>Department of Nuclear Medicine, Klinikum Rechts der Isar, Technische Universität München, Munich, Germany

<sup>7</sup>Department of Radiology, Klinikum Großhadern, Ludwig-Maximilians-Universität München, Munich, Germany

<sup>8</sup>Department of Nuclear Medicine, University of Cologne, Cologne, Germany

The last three authors equally contributed to this work.

## Corresponding author:

Jens Göttler, Department of Neuroradiology, Klinikum Rechts der Isar, TU München, Ismaninger Str. 22, München 81675, Germany.  
 Email: [jens.goettler@tum.de](mailto:jens.goettler@tum.de)

on cerebral blood flow (CBF) and oxygenation changes.<sup>10</sup> Therefore, reduced BOLD-FC in AD might not only reflect changes in neuronal but also in vascular-hemodynamic processes. Correspondingly, reduced neuronal activity indexed by reductions in glucose metabolism (GluMet) approximated by <sup>18</sup>F-fluorodeoxyglucose (FDG)-PET as well as impaired vascular-hemodynamic processes indexed by hypoperfusion estimated by arterial spin labeling (ASL) overlapped remarkably in the pDMN of AD patients.<sup>11,12</sup> Thus, we hypothesized for the pDMN in AD that independently from aberrant neuronal activity, impairments in vascular-hemodynamic processes underlie impairments in BOLD-FC, i.e. that reductions of CBF are specifically linked with decreased connectivity.

To address this hypothesis, we used a hybrid PET/MR scanner to simultaneously acquire resting-state fMRI assessing BOLD-FC, pulsed ASL (pASL), and FDG-PET in patients with AD and healthy controls. Mean BOLD-FC and mean CBF of the pDMN were associated by the use of ANCOVA across all subjects, controlled for mean GluMet.

## Materials and methods

### Participants

Forty-two patients (22 females, age range 52–89 years) and 27 healthy controls (12 females, age range 44–80 years) participated in the study. The ethics committee of the Technische Universität München approved the study, which was conducted in accordance with the principles expressed in the Declaration of Helsinki. All participants provided informed consent. Patients were recruited at the Centre for Cognitive Disorders of the Department of Psychiatry and Psychotherapy of the Technische Universität München, controls by newspaper advertisement. Examination of every participant included medical history, neurological and psychiatric examination, neuropsychological assessment (including mini-mental state examination (MMSE))<sup>13</sup> and an PET/MR scan. Inclusion criterion for patients was the diagnosis of dementia due to probable AD based on the criteria of the National Institutes on Ageing and Alzheimer's Association (NIA-AA).<sup>14</sup> Inclusion criterion for controls was the absence of subjective cognitive impairment. Exclusion criteria for entry into the study were other neurological, psychiatric, or systemic diseases (e.g., vascular dementia, severe depression, schizophrenia and alcoholism) and clinically remarkable structural MRI (e.g. stroke lesions and bleedings) potentially related to cognitive impairment. With special focus on vascular dementia, patients did not have an abrupt onset of symptoms, stepwise symptom deterioration, symptom fluctuations,

a substantial change in personality, a history of strokes, focal neurological symptoms or signs. For 11 patients, we had evidence for atherosclerosis.

Concerning the final sample contributing to results, 10 patients and 5 healthy controls had to be excluded due to motion artifacts (3/2; see Supplementary Material), corrupted data in any imaging modality (4/3), and microbleeds/hemosiderosis possibly associated with cerebral amyloid angiopathy (3/0), resulting in all analyses being conducted on 32 patients and 22 healthy participants (Table 1). Patients' mean MMSE score was  $22.1 \pm 4.2$ , controls showed no relevant cognitive symptoms with MMSE score  $\geq 27$ , mean  $28.6 \pm 1.2$ . All patients were treated with acetylcholinesterase inhibitors and/or NMDA receptor antagonists; 14 patients with AD/11 healthy controls were treated for hypertension (beta-blockers, ACE-inhibitors, and calcium channel blockers), 7/4 for hypercholesterolemia (statins), 2/0 had diabetes mellitus, and 4/4 received antidepressant medication (mirtazapine, citalopram). To estimate cerebral microvascular impairment, the Fazekas score<sup>15</sup> and amount of lacunes were assessed by an experienced neuroradiologist (J.G.), which both did not significantly differ between groups (Table 1). Furthermore, no group difference has been observed for fasting blood glucose levels (Table 1), which have been shown to be associated with cognitive malfunction.<sup>16</sup>

### Data acquisition

Scanning was performed on an integrated 3T Siemens mMR Biograph scanner (Siemens Healthcare, Erlangen, Germany) using the vendor-supplied

**Table 1.** Demographic, neuropsychological and clinical data.

	Patients	Healthy controls	<i>p</i>
N	32	22	
N Female	18	11	0.617
Mean age in years (SD)	65.9 (7.4)	63.6 (7.3)	0.262
Mean education in years (SD)	13.3 (3.8)	12.1 (2.6)	0.266
Mean MMSE (SD)	22.1 (4.2)	28.6 (1.2)	<0.001
Mean Fazekas score (SD)	0.79 (0.83)	0.88 (0.50)	0.699
Mean amount of lacunes (SD)	0.15 (0.46)	0.06 (0.25)	0.494
Mean fasting blood glucose level in mg/dl (SD)	102.8 (19.9)	100.5 (16.5)	0.724

Note: Group comparisons: two-sample *t*-test (age, education, MMSE, Fazekas score, amount of lacunes, fasting glucose level), Chi-square test (sex). MMSE: mini-mental state examination.

12-channel phased-array head coil. Echo-planar-imaging (EPI)-based fMRI, pASL, MP-RAGE, and an FDG-PET volume were acquired within the same session. Additionally, a FLAIR sequence was acquired to screen for brain lesions and abnormalities.

The imaging parameters were as follows:

**EPI.** TR/TE/ $\alpha$  = 2000 ms/30 ms/90°; 35 slices (gap 0.6 mm) covering the whole brain; field of view (FOV) 192 mm; matrix size 64 × 64; voxel size 3.0 × 3.0 × 3.0 mm<sup>3</sup>. Each measurement comprised 240 volumes with interleaved slice acquisitions and a total scan time of 8 min.

**PASL.** For pulsed labeling, we used the proximal inversion with a control for off-resonance effects (PICORE) technique.<sup>17</sup> A single shot EPI readout was used with TR/TE = 2500 ms/13 ms; 11/16 oblique slices (gap 0.6 mm) aligned to posterior structures of the DMN comprising bilateral posterior cingulate cortex, precuneus, inferior parietal lobule, lateral temporal cortex and hippocampus; matrix size 64 × 63, voxel size 4 × 4 × 6 mm<sup>3</sup>. Thin slice periodic saturation pulses were used to obtain a defined bolus (Q2TIPS)<sup>18</sup> using T11/T11S/T12 = 700 ms/1200 ms/1500 ms. Each measurement included 80 pairs of label-control acquisitions and 1 fully relaxed acquisition scan for normalization with a total scan time of 7 min, 20 s.

**MP-RAGE.** TR/TI/TE/ $\alpha$  = 2300 ms/900 ms/2.98 ms/9°; 160 sagittal slices covering the whole brain; FOV 256 mm; matrix size 256 × 256; voxel size 1.0 × 1.0 × 1.0 mm.

**PET.** List-mode acquisition was started 30 min after injection (15 min acquisition time) and comprised 128 slices covering the whole brain; FOV 450 mm; matrix size 192 × 192; voxel size 3.7 × 2.3 × 2.7 mm. Dixon-based attenuation correction was performed as supplied by the scanner manufacturer.

### Data preprocessing

**Overview.** Processing procedures for all modalities followed standard protocols adapted from previous studies for FDG-PET and resting-state fMRI<sup>19</sup> as well as pASL<sup>20,21</sup> using SPM (Wellcome Department of Cognitive Neurology, London, UK) and custom programs written in MATLAB (MathWorks, Natick, MA, USA; see next sections). All parameter maps were normalized to a standard template provided by the Montreal Neurological Institute (MNI) using the same warping parameters. Thereby, we obtained a subject-specific co-registered multimodal dataset of BOLD-FC, quantitative CBF and relative FDG (rFDG)-uptake maps within MNI space and a final

resolution of 3 × 3 × 3 mm<sup>3</sup>. To evaluate the influence of regional atrophy on group differences and ANCOVA results, voxel-based morphometry of MP-RAGE was performed as described previously<sup>22</sup> (see Supplementary Material).

**fMRI data analysis.** fMRI preprocessing steps are described in detail in the Supplementary Material. In brief, realignment, co-registration, normalization to the MNI standard template and smoothing (FWHM Gaussian kernel of 8 × 8 × 8 mm) were conducted using SPM12. Three patients with AD and two healthy controls had to be excluded due to excessive head motion (maximal translation or rotation > 3 mm or 3° and mean translation or rotation > 0.15 mm or 0.1° relative to the previous volume). Movement parameters did not differ between groups. Preprocessed data of all subjects were entered into a group independent component analysis (ICA)<sup>23</sup> using the GIFT toolbox (Medical Imaging Analysis Lab, The Mind Research Network; <http://icatb.sourceforge.net>). ICA decomposes each subject's resting-state fMRI data into statistically independent components. Each component included a spatial map, which reflected that component's z-scored BOLD-FC pattern across space and a time course, which represents the network's activity across time. Only spatial maps of the pDMN and the primary visual network (PVN) were analyzed further as a surrogate of each network's BOLD-FC. While the pDMN was our region-of-interest for the AD specific link between CBF and BOLD-FC, the PVN was used as control region for the specificity of such a link as function of AD pathology effects on the region. The PVN is a representative primary sensory network being at least less impacted by AD pathology than the DMN, particularly in early stages of AD, and it was a component lying within the limited FOV of the pASL sequence.

**PASL data analysis.** Spatial preprocessing and calculation of CBF maps were performed as described previously.<sup>20</sup> In brief, after motion correction, the registered pairs of control and labeled images were subtracted and the 80 difference images were averaged to obtain the perfusion-weighted difference signal  $\Delta S(\text{control-label})$  from the pASL time series. Quantitative CBF maps were then derived according to a general kinetic model,<sup>18</sup> originally introduced by Buxton et al.<sup>24</sup> The model accounts for effects of water exchange between capillaries and tissue and has been adapted to the timing of our sequence.<sup>20</sup> As in our previous work, we used fully relaxed signal in white matter for normalization.<sup>20</sup> ASL-based CBF is principally an absolute measure of cerebral perfusion, and thus we did not apply any intensity normalization when evaluating whether CBF determines BOLD-FC on an absolute scale. CBF maps were

normalised to MNI space and smoothed (FWHM Gaussian kernel of  $8 \times 8 \times 8$  mm).

**FDG-PET data analysis.** FDG-uptake maps were co-registered to the individual MP-RAGE images, normalised to MNI space and scaled by the mean FDG-uptake of the cerebellum.<sup>25</sup> Similar to fMRI and ASL data preprocessing, resulting rFDG-uptake maps were resampled to an isotropic voxel size of  $3 \times 3 \times 3$  mm<sup>3</sup> and smoothed by an FWHM Gaussian kernel of  $8 \times 8 \times 8$  mm. In order to sustain voxel-wise

comparability between all three modalities, we did not apply individual correction for partial volume effects. We rather preferred to evenly control for differences in grey matter density by introducing it as a confounding variable in all analyses.

**Multimodal analysis.** We used pDMN and PVN masks, from a previous study<sup>22</sup> based on an independent sample of healthy elderly, assessed by resting-state fMRI and ICA-based analysis as described above (Figure 1(a)). These masks were used for all further

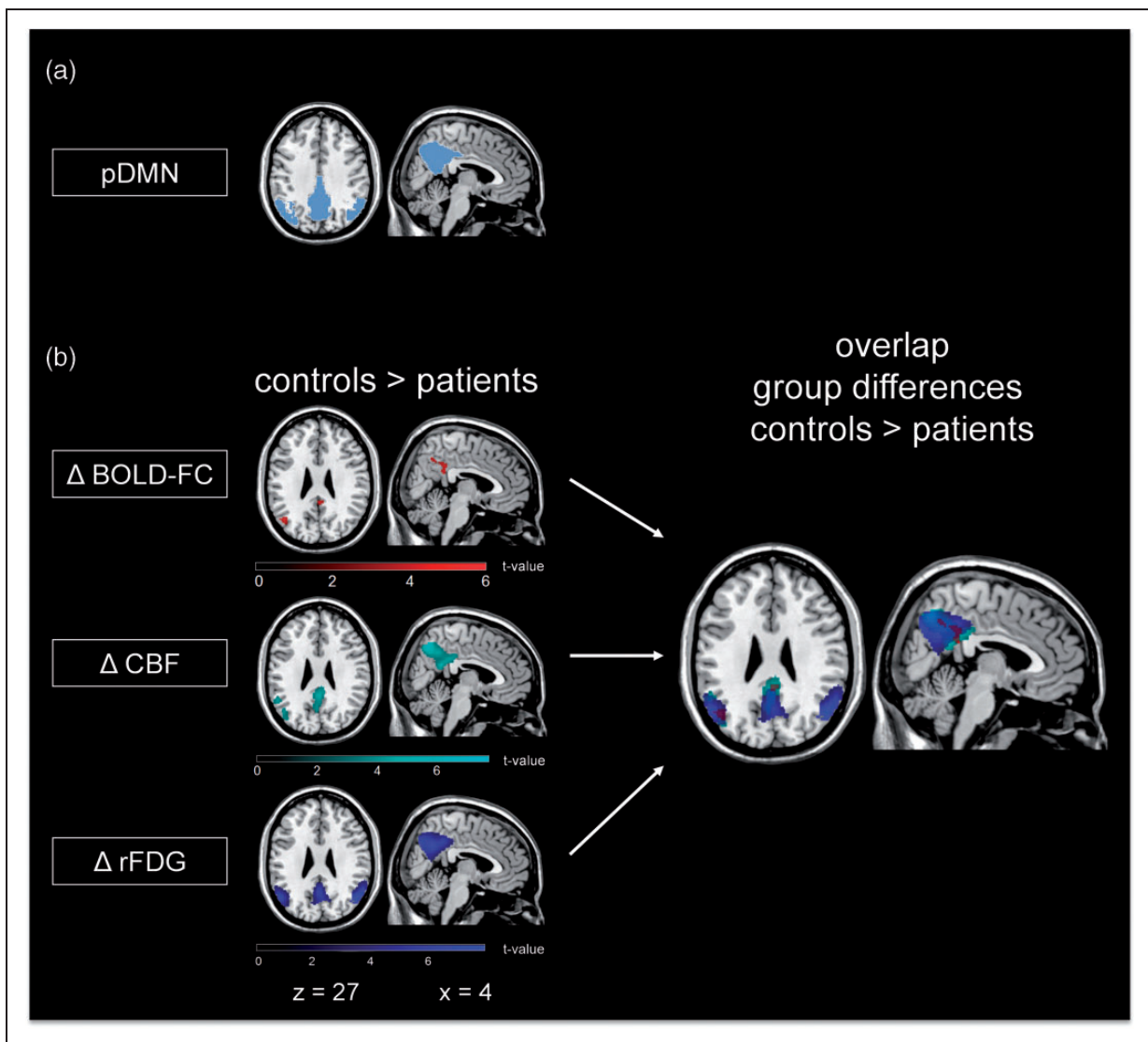


**Figure 1.** Spatial overlap of reduced BOLD-FC, CBF and rFDG-uptake in AD patients compared to healthy controls. (a) ICA-based pDMN mask of an independent sample of healthy elderly. This mask was restricted to grey matter and used for all further group comparisons. (b) Group differences and spatial overlap of areas with reduced BOLD-FC ( $\Delta$  BOLD-FC (red)), CBF ( $\Delta$  CBF (cyan)) and relative FDG-uptake ( $\Delta$  rFDG (blue)) in patients compared to healthy controls are demonstrated by statistical parametric maps (SPM) (two-sample  $t$ -test,  $p < 0.05$  FWE corrected). All SPMs are projected onto a normalized single-subject anatomical T1-weighted data set. pDMN: posterior default mode network; BOLD-FC: blood oxygenation level dependent-functional connectivity; CBF: cerebral blood flow; FDG: <sup>18</sup>F-fluorodeoxyglucose.

statistical analyses. To restrict results to grey matter, group comparisons in all modalities were masked with a user defined grey matter template (probability threshold at 0.5) for all subjects. Mean BOLD-FC, rFDG-uptake and CBF values were extracted from the same grey matter template using MATLAB scripts.

Maps of BOLD-FC, CBF and rFDG-uptake were subjected to a two-sample *t*-test between groups, controlled for age, sex and mean grey matter volume using SPM12.

To test whether absolute baseline blood flow is associated with BOLD-FC in the pDMN/PVN independently of hypometabolism, we conducted an ANCOVA within a univariate general linear model approach as implemented in SPSS23 (IBM, Armonk, NY, USA) with pDMN's/PVN's mean BOLD-FC as the dependent variable. Independent variables were the factors group (patients vs. healthy controls), the pDMN's/PVN's mean CBF, and the interaction of group with mean CBF. To investigate the effects of CBF on BOLD-FC independently from effects of neuronal activity, we adjusted for the effects of pDMN's/PVN's mean rFDG-uptake. In a second step, we added the covariates age, sex and mean grey matter volume within the pDMN/PVN to the ANCOVA model. To analyse the direction of significant interaction effects, Pearson correlation analysis was performed and resulting correlation coefficients were compared between groups using Fisher *r*-to-*z* transformation. To compare group specific effects on mean BOLD-FC of mean CBF and rFDG-uptake, respectively, we replaced the

interaction term of group  $\times$  mean CBF by group  $\times$  mean rFDG-uptake in the ANCOVA model. Finally, to exclude the possibility that differences in the variances of the three measures may have been accountable for the ANCOVA results, we conducted a Levene's test for equal variances.

Furthermore, we performed a voxel-wise multiple linear regression to spatially localize the observed associations of mean BOLD-FC and CBF in patients' pDMN using SPM12. Here, voxel-wise BOLD-FC maps were the dependent variable and mean CBF was the predicting variable, controlling for mean rFDG-uptake.

Significance levels of all clusters of voxel-wise two-sample *t*-tests and voxel-wise multiple regression analysis were set to  $p < 0.05$  FWE corrected,  $k > 50$ . For voxel-wise two-sample *t*-tests, a cluster defining primary threshold of  $p < 0.001$  was used according to Woo et al.<sup>26</sup>

## Results

Patients had lower BOLD-FC in the precuneus/posterior cingulate cortex and the inferior parietal lobule of the pDMN compared to healthy controls (Figure 1(b); Table 2, two-sample *t*-test,  $k > 50$ ,  $p < 0.05$ , FWE corrected). In addition, patients also showed reduced CBF and rFDG-uptake, focusing on the medial and lateral parietal areas of the pDMN, which were overlapping with BOLD-FC reductions in the pDMN (two-sample *t*-test,  $k > 50$ ,  $p < 0.05$  FWE corrected; Figure 1(b); Table 2). No significant CBF and rFDG-uptake

**Table 2.** Group differences in BOLD-FC, CBF and rFDG-uptake within pDMN, controlled for age, sex and atrophy.

Anatomical region	L/R	Cluster	Z-score	T-value	$p$ (FWE corr.)	MNI (x y z)
<b>Two-sample t-test, controls &gt; patients, controlled for age, sex, and atrophy</b>						
<b>BOLD-FC pDMN</b>						
Inferior parietal lobule	R	79	4.43	4.94	0.006	42 -60 42
Posterior cingulate cortex	R	169	4.19	4.63	<0.001	0 -42 34
Posterior cingulate cortex	R		3.96	4.32	<0.001	2 -44 26
Precuneus	R		3.82	3.56	<0.001	6 -58 42
Inferior parietal lobule	L	61	3.90	4.25	0.014	-44 -68 28
<b>CBF</b>						
Precuneus	R	2358	5.71	6.84	<0.001	4 -66 46
Precuneus	L		5.51	6.53	<0.001	-4 -68 46
Inferior parietal lobule	L	1109	5.72q	6.86	0.002	-40 -72 44
<b>rFDG-uptake</b>						
Posterior cingulate cortex	R/L	2215	6.18	7.61	<0.001	0 -58 34
Inferior parietal lobule	L	1178	6.18	7.66	0.001	-50 -66 32
Inferior parietal lobule	R	1548	7.08	9.41	<0.001	44 -68 40
Inferior temporal gyrus	R	177	5.30	6.20	0.045	64 -42 -6

CBF: cerebral blood flow; BOLD-FC: blood oxygenation level dependent functional connectivity; rFDG: relative FDG; pDMN: posterior default mode network; MNI: Montreal Neurological Institute.

group differences have been observed in the temporal lobe in accordance with Chen et al.<sup>11</sup>

The overlap of reductions in all three modalities suggests contributions of hypoperfusion and hypometabolism to BOLD-FC decreases in patients. To test for independency of perfusion effects from hypometabolism, we conducted an ANCOVA of mean BOLD-FC. We found a significant main effect of group ( $p=0.011$ ), confirming the aforementioned group differences in BOLD-FC. Critically, we also found an interaction effect of group  $\times$  mean CBF, indicating that group differences in BOLD-FC are further modulated by baseline pDMN perfusion ( $p=0.024$ ). Pearson correlations supported distinct relations between mean CBF and BOLD-FC for both groups: patients/healthy controls had averaged correlation coefficients of  $r=0.341/-0.328$ ,  $p=0.028/0.068$ , and correlation coefficients were significantly different between groups as tested by the Fisher  $r$ -to- $z$  transformation ( $z=2.36$ ,  $p=0.018$ , Figure 2). As controls showed no significant positive relation between BOLD-FC and perfusion, the interaction effect on BOLD-FC suggests that the positive correlation of BOLD-FC and perfusion is specific for the patient group. Then, to control for potential confounding effects of age, sex, and grey matter

volume in the pDMN, we added corresponding covariates in the ANCOVA model. Again we found a main effect of group ( $p=0.029$ ) and an interaction effect of group  $\times$  mean CBF ( $p=0.045$ ), indicating that our result is not influenced by age, sex, or grey matter volume. Results were not driven by potentially more affected patients with early onset AD ( $<65$ years,  $N=14$ ; Supplementary Material).

Furthermore, no significant interaction effect of group  $\times$  mean rFDG-uptake was observed ( $p=0.608$ ) when replacing the interaction term group  $\times$  mean CBF, suggesting a specific group effect of mean perfusion on mean BOLD-FC. Levene's test found no significant group differences of variances (mean BOLD-FC:  $F=0.058$ ,  $p=0.811$ ; mean CBF:  $F=0.015$ ,  $p=0.902$ ; rFDG-uptake:  $F=2.960$ ,  $p=0.091$ ), supporting reliability of our approach. Furthermore, to estimate the dependence of mean CBF and rFDG-uptake in the ANCOVA model, we performed a correlation analysis for both variables. In line with the literature,<sup>27</sup> mean pDMN's CBF and rFDG-uptake were not significantly correlated (patients:  $r=0.132$ ,  $p=0.236$ ; controls:  $r=-0.121$ ,  $p=0.296$ ), indicating them as independent variables. One should note that intra-individually, voxel-wise CBF and rFDG-uptake

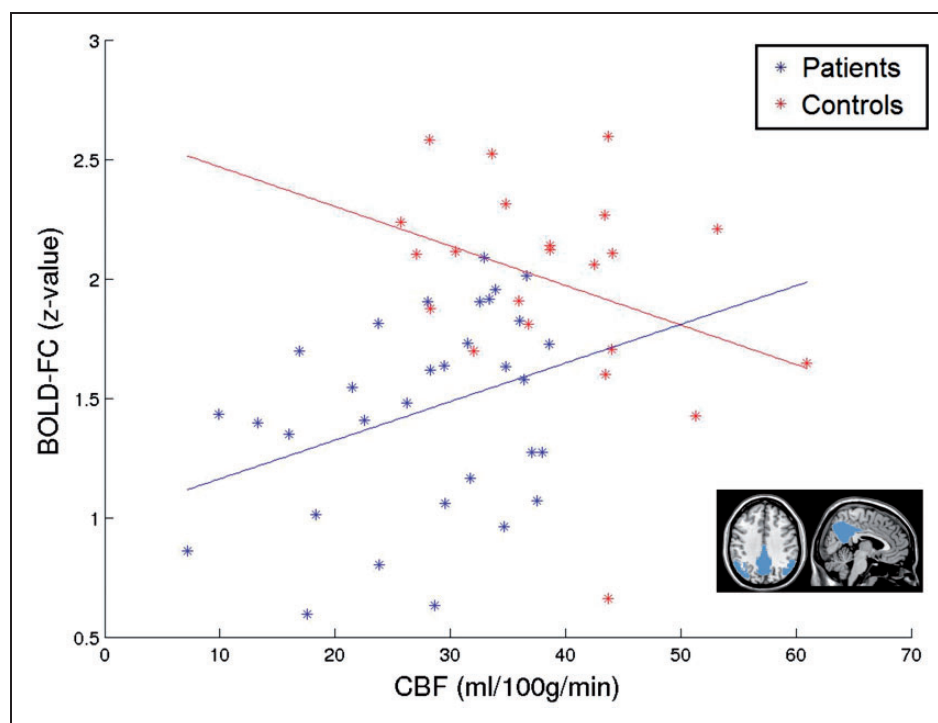


**Figure 2.** AD specific association of mean BOLD-FC with CBF in the pDMN, independently from glucose metabolism. ANCOVA of mean BOLD-FC with the independent variables group and mean CBF (controlled for mean relative FDG-uptake, age, sex, and mean grey matter volume of the pDMN) revealed a significant main effect of group and interaction effect of group  $\times$  mean CBF on BOLD-FC. Scatterplot and correlation between pDMN's mean CBF and mean BOLD-FC to depict interaction effect (patients (blue):  $r=0.341$ ,  $p=0.028$  and healthy controls (red):  $r=-0.328$ ,  $p=0.068$ ).

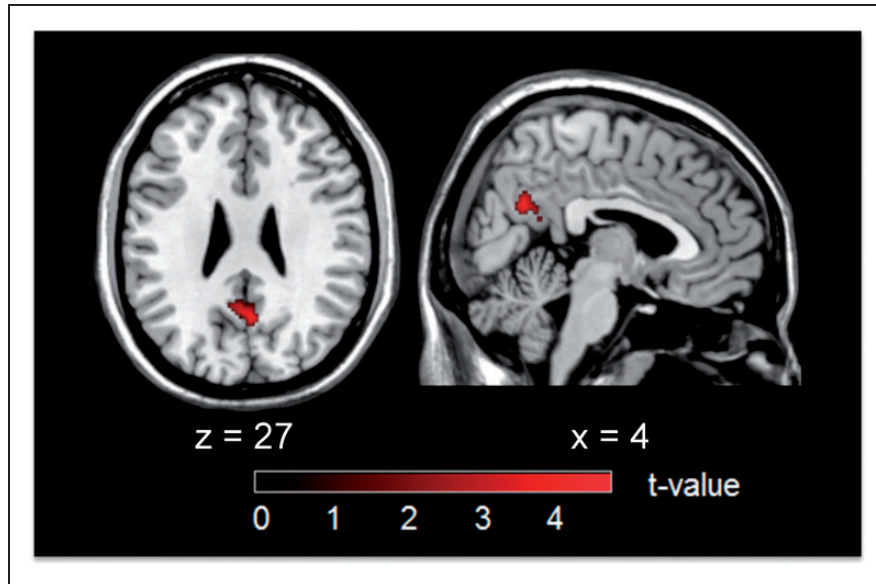


**Figure 3.** Voxel-wise multiple regression of BOLD-FC and pDMN's mean CBF (controlled for mean rFDG-uptake) in patients. Mean CBF in the pDMN was positively associated with BOLD-FC in a cluster in precuneus, independently from mean rFDG-uptake (MNI coordinates 2 -60 28;  $k = 175$ ,  $T = 4.39$ ,  $p = 0.050$  FWE corrected).

were highly correlated across voxels of the pDMN (for detailed description see Supplementary Material and Supplement Figure 1).

To control further for the effect of AD pathology on the AD specific link between CBF and BOLD-FC independent from neuronal activity, we repeated our ANCOVA model analysis for the PVN. The PVN was chosen for two reasons: it was within the FOV of ASL imaging, and it is known to be less affected by AD pathology in early stages of the disease. Accordingly, as tested by two-sample  $t$ -tests, mean CBF, rFDG-uptake, and BOLD-FC were not different across groups. Furthermore, based on the same ANCOVA approach as applied for the pDMN, we did not find significant main effects of group ( $p = 0.922$ ), mean CBF ( $p = 0.868$ ) and interaction effects of group  $\times$  mean CBF ( $p = 0.622$ ) on mean BOLD-FC. This result suggests that GluMet independent perfusion effects on BOLD-FC are specific for the pDMN, and therefore due to the specific impact of AD on pDMN metabolism and perfusion, a function of regional AD effects.

To localize GluMet independent effects of baseline perfusion on BOLD-FC of the pDMN in patients, we conducted a voxel-wise multiple linear regression with BOLD-FC maps as the dependent variable and mean CBF as predicting variables, adjusted for the effects of mean rFDG-uptake. Mean CBF was positively associated with BOLD-FC independently from GluMet in a cluster within the precuneus (MNI coordinates 2 -60 28;  $k = 175$ ,  $T = 4.39$ ,  $p = 0.050$  FWE corrected, Figure 3). This cluster was overlapping with group difference

clusters for CBF, suggesting that group differences in BOLD-FC were further modified by hypoperfusion, particularly in the medial pDMN. Mean rFDG-uptake was not significantly associated with voxel-wise BOLD-FC in the pDMN, indicating that the level of pDMN hypometabolism was not linked with BOLD-FC. To control whether the specific link between BOLD-FC and mean CBF was due to different variance of both regressors mean rFDG-uptake and mean CBF, we analyzed relative standard deviations, indicating how tightly data cluster around the mean. We found small relative standard deviations for both mean rFDG-uptake (0.10) and mean CBF (0.28), supporting the specificity of the association between BOLD-FC and mean CBF.

## Discussion

To test the hypothesis that BOLD-FC reductions in AD reflect changes in vascular-hemodynamic processes independently from decreases in neuronal activity, we assessed patients with AD and healthy controls by simultaneous resting-state fMRI, pASL, and FDG-PET. We found overlapping reductions in BOLD-FC, CBF, and rFDG-uptake in the pDMN of patients, namely the precuneus. Critically, BOLD-FC reductions were correlated with pASL-derived hypoperfusion – independently from FDG-PET-derived glucose hypometabolism, specifically in patients and specifically in the pDMN. These results provide first evidence that impairments of vascular hemodynamic processes

contribute to impaired BOLD-FC in patients with AD, independently from reductions in neuronal activity.

We found reductions in BOLD-FC, CBF and rFDG-uptake within the pDMN, controlling for age, sex and atrophy (Figure 1, Table 2), being in line with a multitude of previous reports.<sup>1–3,20,28</sup> Remarkably, we found that reductions of blood flow and GluMet in patients largely overlapped with BOLD-FC reductions (Figure 1), suggesting a tight coupling between distinct measures, particularly for their decreases in AD. Concerning GluMet, it has been shown previously that metabolism decreases relate with both decreases in blood flow<sup>11,12</sup> and BOLD-FC<sup>29</sup> in AD.

Using ANCOVA of mean BOLD-FC, controlled for rFDG-uptake, we found a significant main effect of group and an interaction effect of group and mean CBF on mean BOLD-FC of the pDMN (Figure 2). Effects were independent from age, sex and atrophy. No corresponding significant interaction effect of group and mean rFDG-uptake on mean BOLD-FC was observed. This means that parts of the variance of the BOLD-FC group differences are explained specifically by baseline CBF reductions independently from GluMet. This finding is specific for AD patients, since only patients showed a significant positive association of mean BOLD-FC with CBF, indicating that baseline pASL-derived CBF reductions are linked with decreased mean BOLD-FC only under conditions of AD, independent of mean FDG-PET-derived hypometabolism. Concerning regional specificity, our finding of a hypometabolism independent positive association of mean CBF and voxel-wise BOLD-FC focuses on the precuneal pDMN (Figures 1 and 3), suggesting complex interaction trajectories among distinct pathophysiological processes in the precuneus. Moreover, perfusion effects on BOLD-FC were specific for the pDMN as confirmed by a control analysis using the PVN in the adjacent occipital cortex. Therefore, our study supports the notion that in AD, vascular-hemodynamic factors disrupt BOLD-FC specifically in parts of the pDMN beyond the effects of reduced neuronal activity.

In fact, vascular lesions are very common in AD; 30–60% of all cases exhibit signs of impaired vascular function such as arterosclerosis, leukoaraiosis, lacunar infarcts, microinfarcts, cerebral amyloid- $\beta$  angiopathy and microbleeds.<sup>30</sup> Most cardiovascular risk factors, such as hypercholesterinaemia, hypertension, and diabetes also increase the risk of developing AD.<sup>31,32</sup> Most interestingly, alterations of vascular hemodynamics were found to precede amyloid- $\beta$  plaque deposition<sup>33</sup> and residuals of such alterations are even regarded as the earliest appearing neuropathological hallmark of AD by some authors.<sup>34,35</sup> Soluble oligomeric amyloid- $\beta$  peptides, main ingredients of amyloid- $\beta$  plaques,

are known to exert synaptotoxic effects and therefore have been proposed to initiate neuronal impairment.<sup>36</sup> There is a mounting body of evidence that vascular changes are one of the factors that seem to induce amyloid- $\beta$  peptide production. Tissue hypoxia and hypoperfusion, for instance, can lead to amyloid- $\beta$  peptide production by activating the enzyme  $\beta$ -secretase.<sup>37,38</sup> Some studies also suggested that amyloid- $\beta$  plaque deposition is promoted in stroke infarction.<sup>39,40</sup> In addition, clearance of amyloid- $\beta$  plaques from the interstitial space has been found to be reduced in AD,<sup>41</sup> which might also be caused by vascular dysfunction.<sup>42</sup> Moreover, amyloid- $\beta$  plaques themselves are known to impair vascular function.<sup>43</sup> In a transgenic mouse model, for instance, reductions of CBF have been demonstrated in regions with overexpression of amyloid- $\beta$  precursor protein by boosting the effects of vasoconstricting factors.<sup>44,45</sup> This condition in turn might induce an accelerated amyloid- $\beta$  accumulation resulting in a vicious cycle of amyloid- $\beta$  accumulation and vascular damage.

In general, BOLD-FC seems to be intimately linked with AD pathology, e.g. BOLD-FC of the pDMN was found to be a predictor for the spatial pattern of amyloid- $\beta$  plaque deposition in individual patients across the spectrum of AD.<sup>7</sup> Although it is well known that the BOLD signal depends on both neuronal and hemodynamic processes,<sup>46,47</sup> changes in BOLD-FC in AD are typically interpreted with regard to changes in neuronal activity only – ignoring potentially relevant hemodynamic contributions. This might partially be due to paradigmatic neuronal-based interpretations of BOLD-FC reductions in AD, such as proposed synaptotoxic effects of amyloid- $\beta$  initiating neuronal impairment.<sup>36</sup> At the same time, amyloid- $\beta$  plaques also impair vascular function as described above. Therefore, our result suggests an additional pathway for changing BOLD-FC, in which amyloid- $\beta$  directly impairs vascular dynamics resulting in aberrant BOLD-FC. Due to the potential relevance of neuronal connectivity for cognitive performance,<sup>22</sup> this pathway might turn out to be interesting for both further pathophysiological and specific intervention-related research. Due to the link between BOLD-FC and amyloid- $\beta$  spread and its potential neuronal impact, a number of further questions are triggered, for example how direct and indirect pathways of amyloid- $\beta$  effects on BOLD-FC interact or depend on vascular integrity.

The current study has several strengths and limitations. First, one strength is the methodologically rigorous approach of simultaneous PET/MR measurement, ensuring that distinct measures derive from the same state of the subject avoiding confounds of serial assessments. Second, limiting is a potential confound induced by hypoperfusion on BOLD-FC detection. It has been



discussed that BOLD-signal amplitude is reduced in hypoperfused brain regions being associated with a lower signal-to-noise ratio, consequently leading to reduced BOLD-FC.<sup>48</sup> We controlled for this potential confound by comparing both temporal signal-to-noise ratio (mean BOLD-signal divided by the temporal standard deviation of BOLD-fluctuations) and variance of precuneus BOLD activity across groups. For both measures, we did not observe significant group differences. Third, BOLD-FC can also be influenced by local reductions in cerebrovascular reactivity, i.e. adaptability, following vasodilatory stimuli, also being associated with hypoperfusion<sup>48,49</sup> and impaired in AD.<sup>50</sup> Therefore, one should note that our phrasing of ‘vascular hemodynamic’ effects on BOLD-FC should indicate that several hemodynamic factors might be relevant for BOLD-FC reductions in AD. Thus, future studies should explicitly test for these factors such as vascular reactivity or oxygenation. Fourth, the limited FOV of the pASL sequence did not include most of the frontal cortex. Consequently, we could not evaluate perfusion effects on networks that are located in this brain region, e.g. the sensorimotor network, salience network and the left and right frontoparietal attention network. However, no significant BOLD-FC and rFDG-uptake decreases were found in these networks, suggesting that the frontal lobe was not severely affected in our study cohort. Fifth, FDG-uptake and ASL are not 100% related to either neuronal or vascular origins, as both physiological measures are strongly related. Both modalities have their shortcomings, such as FDG-uptake being partially perfusion dependent itself<sup>51</sup> and ASL being prone to delayed arterial transit.<sup>52</sup> Especially at the rather short inversion time of 1500 ms, which we employed as a good trade-off between perfusion weighting and a sufficiently high SNR according to literature<sup>20,21,53</sup> we cannot exclude that prolonged arterial transit times (ATT) in elderly individuals might impact CBF measurements as the labeled blood might not have reached the capillaries at the time point of signal read-out yet. This can result in significant signal increases in the pre-capillary arterioles and signal drop-outs especially in typical watershed areas. Increased ATT has been shown to increase variance of CBF-maps and therefore may introduce increased inter-subject variability,<sup>54</sup> which might provide one explanation for the lack of correlation between mean CBF and glucose uptake across subjects, contradicting some PET-based studies.<sup>55,56</sup> Moreover, other inherent technical limitations of either modality (e.g. signal losses due to magnetic field inhomogeneities in fronto-temporal regions in gradient-echo EPI acquisitions in ASL or inaccuracies introduced by MR-based attenuation correction in PET<sup>57</sup>) might further impact correlation between both methods. Indeed, reduced inter-subject correlation of

ASL-CBF and PET-GluMet was found, e.g. in parieto-temporal regions of young subjects, where ATT artifacts are supposed to be less severe.<sup>27</sup> These technical limitations definitely have to be kept in mind when considering our finding that pASL-based perfusion effects on BOLD-FC in AD are independent of FDG-PET-derived glucose metabolism. Additionally, controlling the mean ASL signal by mean rFDG-uptake might regress out some perfusion information. However, as still more variance of BOLD-FC was explained by this rFDG-corrected ASL signal, our procedures reflect rather conservative analyses to assess perfusion effects on BOLD-FC. Lastly, we had a heterogeneous patient group of early and late onset AD patients. However, control analyses provided no evidence that results were strongly driven by either early or late AD onset. Furthermore, as all patients and none of the controls received multiple acetylcholinesterase inhibitors or memantine, medication effects could constitute a confounding factor, which needs to be addressed in future studies.

## Conclusion

We demonstrated that pASL-derived hypoperfusion in the pDMN correlates with impaired BOLD-FC – both independently from FDG-PET-derived glucose hypometabolism and specifically in patients with AD. Results suggest that impairments in vascular-hemodynamic processes distinctively underlie impairments in coherence of BOLD-FC in AD.

## Funding

The author(s) disclosed receipt of the following financial support for the research, authorship, and/or publication of this article: This study was supported by the Faculty of Medicine of the Technische Universität München [grant to JG: KKF E12].

## Declaration of conflicting interests

The author(s) declared the following potential conflicts of interest with respect to the research, authorship, and/or publication of this article: For this article: none. All authors: none. Outside the submitted work: TG reported having received consulting fees from Actelion, Eli Lilly, MSD; Novartis, Quintiles, Roche Pharma, lecture fees from Biogen, Lilly, Parexel, Roche Pharma, and grants to his institution from Actelion and PreDemTech.

## Authors' contributions

Jens Göttler made a substantial contribution to the conception and design, analysis and interpretation of data, and drafted the article.

Christine Preibisch made a substantial contribution to the conception and design, interpretation of data, and drafted the article.

Isabelle Riederer made a substantial contribution to the conception and the acquisition of data, and critically revised the article for important intellectual content.

Lorenzo Pasquini made a substantial contribution to the analysis and interpretation of data, and critically revised the article for important intellectual content.

Panagiotis Alexopoulos made a substantial contribution to the interpretation of data, and critically revised the article for important intellectual content.

Karl Peter Bohn made a substantial contribution to the acquisition and analysis of data, and critically revised the article for important intellectual content.

Igor Yakushev made a substantial contribution to the acquisition and analysis of data, and drafted the article.

Ebba Beller made a substantial contribution to the analysis and interpretation of data, and critically revised the article for important intellectual content.

Stephan Kaczmarz made a substantial contribution to the conception and design, acquisition, analysis and interpretation of data, drafted the article and critically revised it for important intellectual content.

Claus Zimmer made a substantial contribution to the conception and design, and critically revised the article for important intellectual content.

Timo Grimmer made a substantial contribution to the interpretation of data, and critically revised the article for important intellectual content.

Alexander Drzezga made a substantial contribution to the acquisition, analysis and interpretation of data, and critically revised the article for important intellectual content.


Christian Sorg made a substantial contribution to the conception and design, analysis and interpretation of data, and drafted the article.


All authors approved the final version of the manuscript.

### Supplementary material

Supplementary material for this paper can be found at the journal website: <http://journals.sagepub.com/home/jcb>

### ORCID iD

Jens Göttler  <http://orcid.org/0000-0002-5746-2156>.

Christine Preibisch  <http://orcid.org/0000-0003-4067-1928>.

### References

- Sorg C, Riedl V, Muhlau M, et al. Selective changes of resting-state networks in individuals at risk for Alzheimer's disease. *Proc Natl Acad Sci U S A* 2007; 104: 18760–18765.
- Greicius MD, Srivastava G, Reiss AL, et al. Default-mode network activity distinguishes Alzheimer's disease from healthy aging: evidence from functional MRI. *Proc Natl Acad Sci U S A* 2004; 101: 4637–4642.
- Lim HK, Nebes R, Snitz B, et al. Regional amyloid burden and intrinsic connectivity networks in cognitively normal elderly subjects. *Brain* 2014; 137: 3327–3338.
- Zhou J, Gennatas ED, Kramer JH, et al. Predicting regional neurodegeneration from the healthy brain functional connectome. *Neuron* 2012; 73: 1216–1227.
- Myers N, Pasquini L, Gottler J, et al. Within-patient correspondence of amyloid-beta and intrinsic network connectivity in Alzheimer's disease. *Brain* 2014; 137: 2052–2064.
- Busche MA and Konnerth A. Impairments of neural circuit function in Alzheimer's disease. *Philos Trans R Soc Lond B Biol Sci* 2016; 371: 20150429.
- Pasquini L, Benson G, Grothe MJ, et al. Individual correspondence of amyloid-beta and intrinsic connectivity in the posterior default mode network across stages of Alzheimer's disease. *J Alzheimers Dis* 2017; 58: 763–773.
- Buckner RL, Andrews-Hanna JR and Schacter DL. The brain's default network: anatomy, function, and relevance to disease. *Ann N Y Acad Sci* 2008; 1124: 1–38.
- Raichle ME. The brain's default mode network. *Annu Rev Neurosci* 2015; 38: 433–447.
- Buxton RB, Uludag K, Dubowitz DJ, et al. Modeling the hemodynamic response to brain activation. *Neuroimage* 2004; 23(Suppl 1): S220–S233.
- Chen Y, Wolk DA, Reddin JS, et al. Voxel-level comparison of arterial spin-labeled perfusion MRI and FDG-PET in Alzheimer disease. *Neurology* 2011; 77: 1977–1985.
- Musiek ES, Chen Y, Korczykowski M, et al. Direct comparison of fluorodeoxyglucose positron emission tomography and arterial spin labeling magnetic resonance imaging in Alzheimer's disease. *Alzheimers Dement* 2012; 8: 51–59.
- Folstein MF, Folstein SE and McHugh PR. "Mini-mental state". A practical method for grading the cognitive state of patients for the clinician. *J Psychiatr Res* 1975; 12: 189–198.
- McKhann GM, Knopman DS, Chertkow H, et al. The diagnosis of dementia due to Alzheimer's disease: recommendations from the National Institute on Aging-Alzheimer's Association workgroups on diagnostic guidelines for Alzheimer's disease. *Alzheimers Dement* 2011; 7: 263–269.
- Fazekas F, Chawluk JB, Alavi A, et al. MR signal abnormalities at 1.5 T in Alzheimer's dementia and normal aging. *Am J Roentgenol* 1987; 149: 351–356.
- Mortby ME, Janke AL, Anstey KJ, et al. High "normal" blood glucose is associated with decreased brain volume and cognitive performance in the 60s: the PATH through life study. *PLoS One* 2013; 8: e73697.
- Wong EC, Buxton RB and Frank LR. Implementation of quantitative perfusion imaging techniques for functional brain mapping using pulsed arterial spin labeling. *NMR Biomed* 1997; 10: 237–249.
- Luh WM, Wong EC, Bandettini PA, et al. QUIPSS II with thin-slice T1 periodic saturation: a method for improving accuracy of quantitative perfusion imaging using pulsed arterial spin labeling. *Magn Reson Med* 1999; 41: 1246–1254.
- Riedl V, Utz L, Castrillon G, et al. Metabolic connectivity mapping reveals effective connectivity in the resting

- human brain. *Proc Natl Acad Sci U S A* 2016; 113: 428–433.
20. Preibisch C, Sorg C, Forschler A, et al. Age-related cerebral perfusion changes in the parietal and temporal lobes measured by pulsed arterial spin labeling. *J Magn Reson Imaging* 2011; 34: 1295–1302.
  21. Alexopoulos P, Sorg C, Forschler A, et al. Perfusion abnormalities in mild cognitive impairment and mild dementia in Alzheimer's disease measured by pulsed arterial spin labeling MRI. *Eur Arch Psychiatry Clin Neurosci* 2012; 262: 69–77.
  22. Koch K, Myers NE, Gottler J, et al. Disrupted intrinsic networks link amyloid-beta pathology and impaired cognition in prodromal Alzheimer's disease. *Cereb Cortex* 2015; 25: 4678–4688.
  23. Calhoun VD, Adali T, Pearlson GD, et al. Spatial and temporal independent component analysis of functional MRI data containing a pair of task-related waveforms. *Hum Brain Mapp* 2001; 13: 43–53.
  24. Buxton RB, Frank LR, Wong EC, et al. A general kinetic model for quantitative perfusion imaging with arterial spin labeling. *Magn Reson Med* 1998; 40: 383–396.
  25. Dukart J, Mueller K, Horstmann A, et al. Differential effects of global and cerebellar normalization on detection and differentiation of dementia in FDG-PET studies. *Neuroimage* 2010; 49: 1490–1495.
  26. Woo CW, Krishnan A and Wager TD. Cluster-extent based thresholding in fMRI analyses: pitfalls and recommendations. *Neuroimage* 2014; 91: 412–419.
  27. Cha YH, Jog MA, Kim YC, et al. Regional correlation between resting state FDG PET and pCASL perfusion MRI. *J Cereb Blood Flow Metab* 2013; 33: 1909–1914.
  28. Foster NL, Chase TN, Fedio P, et al. Alzheimer's disease: focal cortical changes shown by positron emission tomography. *Neurology* 1983; 33: 961–965.
  29. Drzezga A, Becker JA, Van Dijk KR, et al. Neuronal dysfunction and disconnection of cortical hubs in nondemented subjects with elevated amyloid burden. *Brain* 2011; 134: 1635–1646.
  30. Jellinger KA. Pathology and pathogenesis of vascular cognitive impairment—a critical update. *Front Aging Neurosci* 2013; 5: 17.
  31. Luchsinger JA and Mayeux R. Cardiovascular risk factors and Alzheimer's disease. *Curr Atheroscler Rep* 2004; 6: 261–266.
  32. Mayeux R. Epidemiology of neurodegeneration. *Annu Rev Neurosci* 2003; 26: 81–104.
  33. Iturria-Medina Y, Sotero RC, Toussaint PJ, et al. Early role of vascular dysregulation on late-onset Alzheimer's disease based on multifactorial data-driven analysis. *Nat Commun* 2016; 7: 11934.
  34. Hardy JA and Higgins GA. Alzheimer's disease: the amyloid cascade hypothesis. *Science* 1992; 256: 184–185.
  35. Hardy J and Selkoe DJ. The amyloid hypothesis of Alzheimer's disease: progress and problems on the road to therapeutics. *Science* 2002; 297: 353–356.
  36. Walsh DM and Selkoe DJ. Deciphering the molecular basis of memory failure in Alzheimer's disease. *Neuron* 2004; 44: 181–193.
  37. Kitaguchi H, Tomimoto H, Ihara M, et al. Chronic cerebral hypoperfusion accelerates amyloid beta deposition in APPSwInd transgenic mice. *Brain Res* 2009; 1294: 202–210.
  38. Sun X, He G, Qing H, et al. Hypoxia facilitates Alzheimer's disease pathogenesis by up-regulating BACE1 gene expression. *Proc Natl Acad Sci U S A* 2006; 103: 18727–18732.
  39. Ly JV, Rowe CC, Villemagne VL, et al. Subacute ischemic stroke is associated with focal 11C PiB positron emission tomography retention but not with global neocortical Aβ deposition. *Stroke* 2012; 43: 1341–1346.
  40. Jendroska K, Poewe W, Daniel SE, et al. Ischemic stress induces deposition of amyloid beta immunoreactivity in human brain. *Acta Neuropathol* 1995; 90: 461–466.
  41. Mawuenyega KG, Sigurdson W, Ovod V, et al. Decreased clearance of CNS beta-amyloid in Alzheimer's disease. *Science* 2010; 330: 1774.
  42. Iadecola C. The pathobiology of vascular dementia. *Neuron* 2013; 80: 844–866.
  43. Zlokovic BV. Neurovascular mechanisms of Alzheimer's neurodegeneration. *Trends Neurosci* 2005; 28: 202–208.
  44. Iadecola C, Zhang F, Niwa K, et al. SOD1 rescues cerebral endothelial dysfunction in mice overexpressing amyloid precursor protein. *Nat Neurosci* 1999; 2: 157–161.
  45. Niwa K, Porter VA, Kazama K, et al. A beta-peptides enhance vasoconstriction in cerebral circulation. *Am J Physiol Heart Circ Physiol* 2001; 281: H2417–H2424.
  46. Mark CI, Mazerolle EL and Chen JJ. Metabolic and vascular origins of the BOLD effect: implications for imaging pathology and resting-state brain function. *J Magn Reson Imaging* 2015; 42: 231–246.
  47. Liu TT. Neurovascular factors in resting-state functional MRI. *Neuroimage* 2013; 80: 339–348.
  48. Liu P, Hebrank AC, Rodrigue KM, et al. A comparison of physiologic modulators of fMRI signals. *Hum Brain Mapp* 2013; 34: 2078–2088.
  49. Golestani AM, Wei LL and Chen JJ. Quantitative mapping of cerebrovascular reactivity using resting-state BOLD fMRI: validation in healthy adults. *Neuroimage* 2016; 138: 147–163.
  50. Cantin S, Villien M, Moreaud O, et al. Impaired cerebral vasoreactivity to CO<sub>2</sub> in Alzheimer's disease using BOLD fMRI. *Neuroimage* 2011; 58: 579–587.
  51. Alf MF, Duarte JM, Schibli R, et al. Brain glucose transport and phosphorylation under acute insulin-induced hypoglycemia in mice: an 18F-FDG PET study. *J Nucl Med* 2013; 54: 2153–2160.
  52. Alsop DC, Detre JA, Golay X, et al. Recommended implementation of arterial spin-labeled perfusion MRI for clinical applications: a consensus of the ISMRM perfusion study group and the European consortium for ASL in dementia. *Magn Reson Med* 2015; 73: 102–116.
  53. Trebesch S, Riederer I, Preibisch C, et al. Diagnostic potential of pulsed arterial spin labeling in Alzheimer's disease. *Front Neurosci* 2016; 10: 154.
  54. Mutsaerts HJ, Petr J, Vaclavu L, et al. The spatial coefficient of variation in arterial spin labeling cerebral blood flow images. *J Cereb Blood Flow Metab* 2017; 37: 318–43192.

55. Paulson OB, Hasselbalch SG, Rostrup E, et al. Cerebral blood flow response to functional activation. *J Cereb Blood Flow Metab* 2010; 30: 2–14.
56. Rodriguez-Vieitez E, Leuzy A, Chiotis K, et al. Comparability of [18F]THK5317 and [11C]PIB blood flow proxy images with [18F]FDG positron emission tomography in Alzheimer's disease. *J Cereb Blood Flow Metab* 2017; 37: 740–749.
57. Ladefoged CN, Law I, Anazodo U, et al. A multi-centre evaluation of eleven clinically feasible brain PET/MRI attenuation correction techniques using a large cohort of patients. *Neuroimage* 2017; 147: 346–359.